Dendritic connectivity controls biodiversity patterns in experimental metacommunities

Francesco Carrara[a,1], Florian Altermatt[b,1,2], Ignacio Rodriguez-Iturbe[c], and Andrea Rinaldo[a,d,2]

[a]Laboratory of Ecohydrology (ECHO/IEE/ENAC), École Polytechnique Fédérale Lausanne, 1015 Lausanne, Switzerland; [b]Department of Aquatic Ecology, Eawag: Swiss Federal Institute of Aquatic Science and Technology, 8600 Dübendorf, Switzerland; [c]Department of Civil and Environmental Engineering, Princeton University, Princeton, NJ 08544; and [d]Dipartimento di Ingegneria Civile, Edile ed Ambientale, Università di Padova, 35131 Padova, Italy

Edited by Stephen R. Carpenter, University of Wisconsin, Madison, WI, and approved February 21, 2012 (received for review November 30, 2011)

Biological communities often occur in spatially structured habitats where connectivity directly affects dispersal and metacommunity processes. Recent theoretical work suggests that dispersal constrained by the connectivity of specific habitat structures, such as dendrites like river networks, can explain observed features of biodiversity, but direct evidence is still lacking. We experimentally show that connectivity per se shapes diversity patterns in microcosm metacommunities at different levels. Local dispersal in isotropic lattice landscapes homogenizes local species richness and leads to pronounced spatial persistence. On the contrary, dispersal along dendritic landscapes leads to higher variability in local diversity and among-community composition. Although headwaters exhibit relatively lower species richness, they are crucial for the maintenance of regional biodiversity. Our results establish that spatially constrained dendritic connectivity is a key factor for community composition and population persistence.

microbial microcosms | directional dispersal | community assembly | nonneutral dynamics

A major aim of community ecology is to identify processes that define large-scale biodiversity patterns (1–8). For simplified landscapes, often described geometrically by linear or lattice structures, a variety of local environmental factors have been brought forward as the elements creating and maintaining diversity among habitats (9–12). Many highly diverse landscapes, however, exhibit hierarchical spatial structures that are shaped by geomorphological processes and neither linear nor 2D environmental matrices may be appropriate to describe biodiversity of species living within dendritic ecosystems (13, 14). Furthermore, in many environments intrinsic disturbance events contribute to spatiotemporal heterogeneity (14, 15). Riverine ecosystems, among the most diverse habitats on earth (16), represent an outstanding example of such mechanisms (7, 17–19).

Here, we investigate the effects of directional dispersal imposed by the habitat-network structure on the biodiversity of metacommunities (MCs), by conducting a laboratory experiment using aquatic microcosms. Experiments were conducted in 36-well culture plates (Fig. 1), thus imposing by construction a metacommunity structure (20, 21): Each well hosted a local community (LC) within the whole landscape and dispersal occurred by periodic transfer of culture medium among connected LCs (22), following two different geometries (*Materials and Methods*, Fig. S1, and *SI Materials and Methods*). We compared spatially heterogeneous MCs following a river network (RN) geometry (Fig. 1*D*), with spatially homogeneous MCs, in which every LC has a 2D lattice of four nearest neighbors (2D) (Fig. 1*E*). The coarse-grained RN landscape is derived from a scheme (13) known to reproduce the scaling properties observed in real river systems (Fig. 1*A*).

To single out the effects of connectivity, we deliberately avoided reproducing other geomorphic features of real river networks, such as the bias in downstream dispersal, the growing habitat capacity with accumulated contributing area, or other environmental conditions connected to topographic elevation. Directional dispersal refers to the pathway constrained by the habitat connectivity and does not imply downstream-biased dispersal kernels; that is, in all treatments dispersal kernels were identical and symmetric. Disturbance consisted of medium replacement and reflects the spatial environmental heterogeneity inherent to many natural systems (*Materials and Methods*).

The microcosm communities were composed of nine protozoan and one rotifer species, which are naturally co-occurring in freshwater habitats, with bacteria as a common food resource (21). These species cover a wide range of body sizes (Fig. 1*B*), intrinsic growth rates, and other important biological traits (23) (Table S1). Thus, the microcosm communities cover substantial biological complexity in terms of more structured trophic levels and species interactions that cannot be entirely captured by any model (24) (*Materials and Methods* and *SI Materials and Methods*). Previous microbial experiments found that spatiotemporal heterogeneity among local communities induced by disturbance (25) and dispersal (26–28) events has a strong influence on species coexistence and biodiversity. In previous works (20, 22, 26, 28) the focus was mostly on dispersal distance, dispersal rates, and dispersal kernels and how they affect diversity patterns in relatively simple landscapes. These factors, directly affecting the history of community assembly (29, 30), introduce variability in community composition in terms of abundances and local species richness. We specifically studied basic mechanisms of dispersal and landscape structure on diversity patterns in metacommunities mimicking realistic network structures. Thus, our replicated and controlled experimental design sheds light on the role of connectivity in more structured metacommunities, disentangling complex natural systems' behavior (31).

Results and Discussion

We compared the RN and the 2D landscapes, focusing on three measures of biodiversity: the number of species present in a local community (α-diversity), among-community diversity (β-diversity), and the number of LCs in which a given species is present (species occupancy) (7). We found a significantly broader α-diversity distribution (Figs. 2 and 3 *A* and *B*) in the RN compared with the 2D landscapes [measured as the coefficient of variation (CV), $\overline{\mathrm{CV}}_{\mathrm{RN}} = 0.265$, $\overline{\mathrm{CV}}_{\mathrm{2D}} = 0.122$, paired t test, $t_5 = 7.05$, $P = 0.0009$). Furthermore β-diversity, here described by the spatial decay of Jaccard's similarity index (*Materials and Methods* and *SI Materials and Methods*), was higher in the RN compared with the 2D landscapes (Fig. 3*C*). Mean local species richness in RN was significantly lower compared with that in 2D landscapes

Author contributions: F.C., F.A., I.R.-I., and A.R. designed research; F.C. and F.A. performed research; F.C. and F.A. analyzed data; and F.C., F.A., I.R.-I., and A.R. wrote the paper.

The authors declare no conflict of interest.

This article is a PNAS Direct Submission.

Freely available online through the PNAS open access option.

[1]F.C. and F.A. contributed equally to this work.

[2]To whom correspondence may be addressed. E-mail: florian.altermatt@eawag.ch or andrea.rinaldo@epfl.ch.

This article contains supporting information online at www.pnas.org/lookup/suppl/doi:10.1073/pnas.1119651109/-/DCSupplemental.

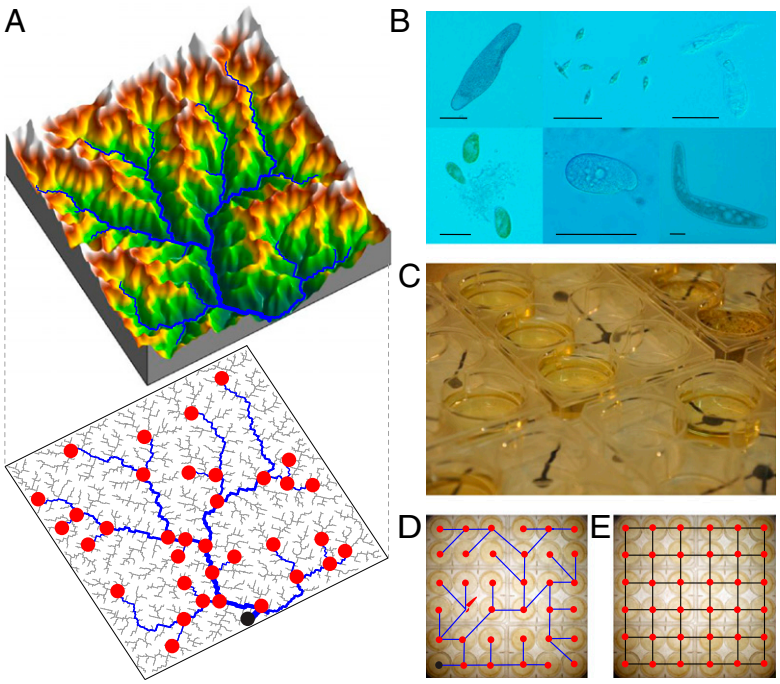

Fig. 1. Design of the connectivity experiment. (*A*) The river network (RN) landscape (*Lower*: red points label the position of LCs, and the black point is the outlet) derives from a coarse-grained optimal channel network (OCN) that reflects the 3D structure of a river basin (*Upper*). (*B–E*) The microcosm experiment involves protozoan and rotifer species. (*B*) Subset of the species (for names see *SI Materials and Methods*). (Scale bars, 100 μm.) (*C*) Communities were kept in 36-well plates. (*D* and *E*) Dispersal to neighboring communities follows the respective network structure: blue lines are for RN (*D*), same network as in *A*, and black lines are for 2D lattice with four nearest neighbors (*E*).

(Fig. 2 *A–D*, $\overline{\langle\alpha\rangle}_{RN} = 5.72$, $\overline{\langle\alpha\rangle}_{2D} = 6.72$, paired t test, $t_5 = 9.23$, $P = 0.0003$). These results confirm theoretical predictions on the role of directional dispersal from both individual- and metacommunity-based models (7, 32, 33). Specifically, we experimentally observe that the anisotropy induced by directional dispersal has a strong impact on the spatial configuration of the species occupancy, reflected in α- and β-diversity (Figs. 2 *A–D* and 3*E*). Anisotropy results in radically different distributions of closeness centrality, i.e., the mean geometric geodesic distance (34) and the mean distance l between all LC pairs (Fig. S2) in RN vs. 2D landscapes ($l_{RN} = 5.33$, $l_{2D} = 3$) (*SI Materials and Methods*).

In parallel to the experiment we developed a stochastic model, generalizing across spatial and temporal scales (*Materials and Methods*). The model embeds spatiotemporal environmental heterogeneity and is based on a Lotka–Volterra competition model. We simulated the dynamics of species competing for space and food resources on the same trophic level, subjected to periodic perturbation events consisting of partial habitat destruction. The model is an approximation to our experimental system, but does not contain trophic dynamics that may occur in the protozoa communities. Dispersal to neighboring patches can generate recolonization.

We measured species-specific intrinsic growth rates and carrying capacities in pure cultures (Fig. S3 and Table S1), and we used these specific values in the stochastic model, without fitting parameters (*Materials and Methods*). Even if estimates on growth rates and carrying capacities were already available for some species (21), we repeated these experiments to get direct values for our specific experimental conditions, i.e., illumination, nutrient levels, chamber temperature, and particular environment provided by well plates (volume and ratio of area to volume). The model confirmed the experimental observations: a higher variability for α-diversity (Fig. 2 *E* and *F*) and a higher β-diversity (Fig. 3*C*) in dendrites compared with lattice landscapes. These patterns were robust over a long time interval relative to species-intrinsic growth rates (Fig. 3*D*, Fig. S4, and *SI Materials and Methods*). Furthermore, the patterns are consistent also at different spatial scales (Fig. 3*D*).

The bimodal shape of the α-diversity distribution observed in both model and experiment for the river network geometry (Fig. 3*A*) called for an analysis based on the degree of connectivity, d, which gives the number of connected neighboring nodes to a LC. In the "headwater" (H) class, LCs have $d_H = 1$ and are connected uniquely to their "downstream" node whereas in the "confluence" (C) class, LCs are characterized by $d_C = 3$ and are connected to two "upstream" and one downstream nodes. In our scenario, the terms downstream and upstream refer only to the position of the connected LC with respect to the outlet. They do not refer to a mass flow as dispersal is not directionally biased (7) (*Materials and Methods*). The outlet (O) of the network, connected only to its upstream node ($d_O = 1$), falls into the H class.

We found that the α-diversity distribution for Hs peaks at a significantly lower value compared with the peak of the Cs' distribution ($\overline{\langle\alpha\rangle}_H = 5.29$, $\overline{\langle\alpha\rangle}_C = 6.10$, paired t test, $t_5 = 7.24$, $P = 0.0008$; Fig. S5) and exhibits higher variability (Fig. 4*A*). Fig. 2 *A* and *E* shows this pattern, in which the backbone of the river network exhibits on average a higher species richness with respect to peripheral communities.

To explain the variability of the local species richness in the RN, we included two other factors in our analysis: the "ecological diameter" l_i of the LC i (strictly related to its closeness centrality) and the temporal distribution of disturbance events. The ecological diameter is simply defined as the average distance $l_i = \langle d_{ij}\rangle_j$ of i from all of the other LCs j in the RN, where d_{ij} represents the shortest (geodesic) distance between i and j (34). We found that connectivity significantly affected α-diversity in the RN landscape (ANOVA, $F_{1,5} = 12.09$, $P = 0.0006$), whereas neither time to the last disturbance nor network centrality significantly affected local species richness (ANOVA, $F_{6,5} = 1.66$, $P = 0.13$; and $F_{4,5} = 0.71$, $P = 0.59$) (Fig. S6 and *SI Materials and Methods*).

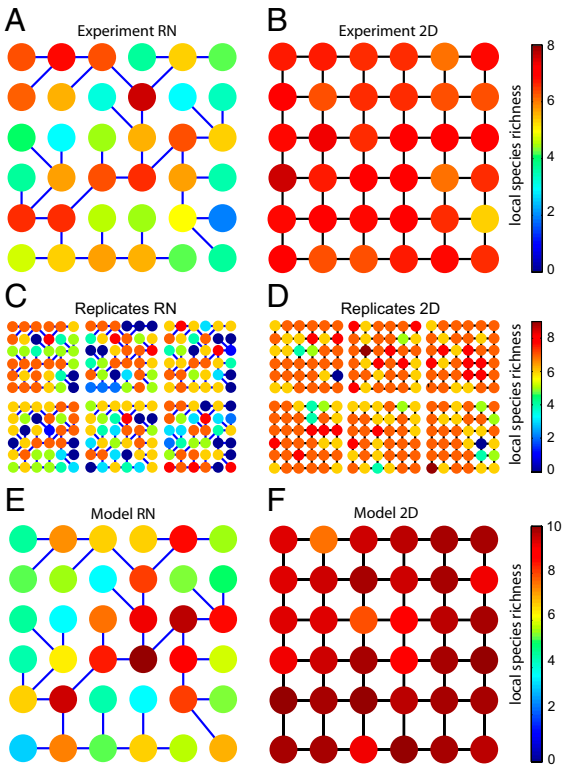

Fig. 2. Experimental and theoretical local species richness in river network (RN) and lattice (2D) landscapes. (*A* and *B*) Mean local species richness (α-diversity, color coded; every dot represents a LC) for the microcosm experiment averaged over the six replicates. (*C* and *D*) Species richness for each of these replicates individually. (*E* and *F*) The stochastic model predicts similar mean α-diversity patterns (note different scales).

We obtained β-diversity separately for headwaters and confluences, to test the difference in species composition within the river network structure. Headwaters exhibit not only a higher variability in α-diversity, but also a higher β-diversity compared with confluences (Fig. 4*B*), confirming patterns found in natural river basins (16, 18). Therefore, the difference in the loss of spatial correlation relative to lattice landscapes appeared even higher when only headwaters were considered in the comparison. These results reveal the crucial importance of headwaters as a source of biodiversity for the whole landscape. In natural systems other local environmental factors may play a role in structuring ecosystems (35). Nevertheless, our causal approach sheds light on the sole effect of directional dispersal on biodiversity. Note that the patterns we found in river network geometry are predicted to be even stronger in the presence of a downstream dispersal, which is typical for many passively transported riparian and aquatic species in river basins (19, 33).

We observed a lower mean α-diversity in the experiment compared with the theoretical predictions ($\Delta\overline{\langle\alpha\rangle}_{RN} = 37\%$, $\Delta\overline{\langle\alpha\rangle}_{2D} = 42\%$), but a rescaling to the experimental mean produced a consistent local species richness distribution (Fig. 3 *A* and *B*). Species occupancies are presented in Fig. 3*E* as a rank-occupancy curve: Both the model and the experiment revealed that well-connected 2D landscapes presented higher spatial persistence compared with river network environments, but the sharp decrease in experimental rank-occupancy curves observed in both landscapes suggests that some species are disadvantaged. It is likely that species competition in the experiment had stronger effects on the persistence of weaker species than that generated in the model by pure competition for space (*SI Materials and Methods*).

At this point of the discussion the following question arises: How does the system react over these spatiotemporal scales, without any disturbance–dispersal events? We tested species' ability to coexist in an "isolation" treatment, under the same environmental conditions (*Materials and Methods*). We hypothesized that under stress (space saturation and reduced availability of bacteria) larger protozoans, such as *Blepharisma* and *Spirostomum* sp., could predate on smaller protozoans, such as *Chilomonas*, *Tetrahymena*, and *Colpidium* sp. (Table S1 for species' traits). The latter appeared to be strongly inferior competitors (Fig. S6). Note that predation could happen even at low protist densities and high bacterial densities.

We found that a consistent subset of four species survived at the end of the isolation experiment (Fig. S7), whereas all other species went mostly extinct, resulting in lower values of both α- and β-diversity ($\overline{CV}_{Isolation} = 0.086$, $\overline{\langle\alpha\rangle}_{Isolation} = 4.17$). The results confirmed the importance of dispersal and connectivity for maintaining higher levels of biodiversity observed in fragmented landscapes (Fig. 4*A*) (36, 37), at temporal scales over which competitive exclusion dynamics have emerged in isolated communities. Clearly, competition, although stronger than just for space and resources, has not altered the connectivity-induced patterns highlighted by both the theoretical and the experimental approaches.

Because the types of dispersal and disturbances used in our system are not specific to riverine environments, the above results apply to a variety of heterogeneous and fragmented environments. We suggest that species constrained to disperse within dendritic corridors face reduced spatial persistence and higher extinction risks. On the other hand, heterogeneous habitats sustain higher levels of among-community biodiversity that can be altered by modifying the connectivity of the system, with implications for community ecology and conservation biology.

Materials and Methods

Aquatic Communities. Each LC within a MC was initialized with nine protozoan species, one rotifer species, and a set of common freshwater bacteria as a food resource. The nine protozoan species were *Blepharisma* sp., *Chilomonas* sp., *Colpidium* sp., *Euglena gracilis*, *Euplotes aediculatus*, *Paramecium aurelia*, *Paramecium bursaria*, *Spirostomum* sp. and *Tetrahymena* sp., and the rotifer was *Cephalodella* sp.). *Blepharisma* sp., *Chilomonas* sp., and *Tetrahymena* sp. were supplied by Carolina Biological Supply, whereas all other species were originally isolated from a natural pond (38) and have also been used for other studies (21, 22). We use the same nomenclature as in such studies, except for *Cephalodella* sp., which has been previously identified as *Rotaria* sp. All species are bacterivores whereas *E. gracilis, E. aediculatus*, and *P. bursaria* can also photosynthesize. Furthermore, *Blepharisma* sp., *Euplotes aediculatus*, and *Spirostomum* sp. may not only feed on bacteria but also can predate on smaller flagellates. Twenty-four hours before inoculation with protozoans and rotifer, three species of bacteria (*Bacillus cereus*, *Bacillus subtilis*, and *Serratia marcescens*) were added to each community. LCs were located in 10-mL multiwell culture plates containing a solution of sterilized local spring water, 1.6 $g{\cdot}L^{-1}$ of soil, and 0.45 $g{\cdot}L^{-1}$ of Protozoan Pellets (Carolina Biological Supply). Protozoan Pellets and soil provide nutrients for bacteria, which are consumed by protozoans. We conducted the experiment in a climatized room at 21 °C under constant fluorescent light. On day 0, 100 individuals of each species were added, except for *E. gracilis* (500 individuals) and *Spirostomum* (40 individuals), which naturally occur, respectively, at higher and lower densities. We determined species' intrinsic growth rate *r* and carrying capacity *K* in pure cultures, at identical conditions (*Species' Traits: Population Growth* below).

Landscapes. Each MC consisted of 36 LCs, connected according to two different schemes: a lattice network in which each LC has four nearest neighbors with periodic boundaries (2D landscape) and a coarse-grained RN structure, obtained from a 200 × 200 space filling optimal channel network (OCN) (13, 39, 40), with an appropriate threshold on the drainage area (*SI Materials and Methods*). In the RN landscape a LC has either three nearest neighbors (C) or one nearest neighbor (H). Landscapes of these two dispersal treatments were replicated six times. Furthermore, we had MCs of the isolation treatment, replicated three times.

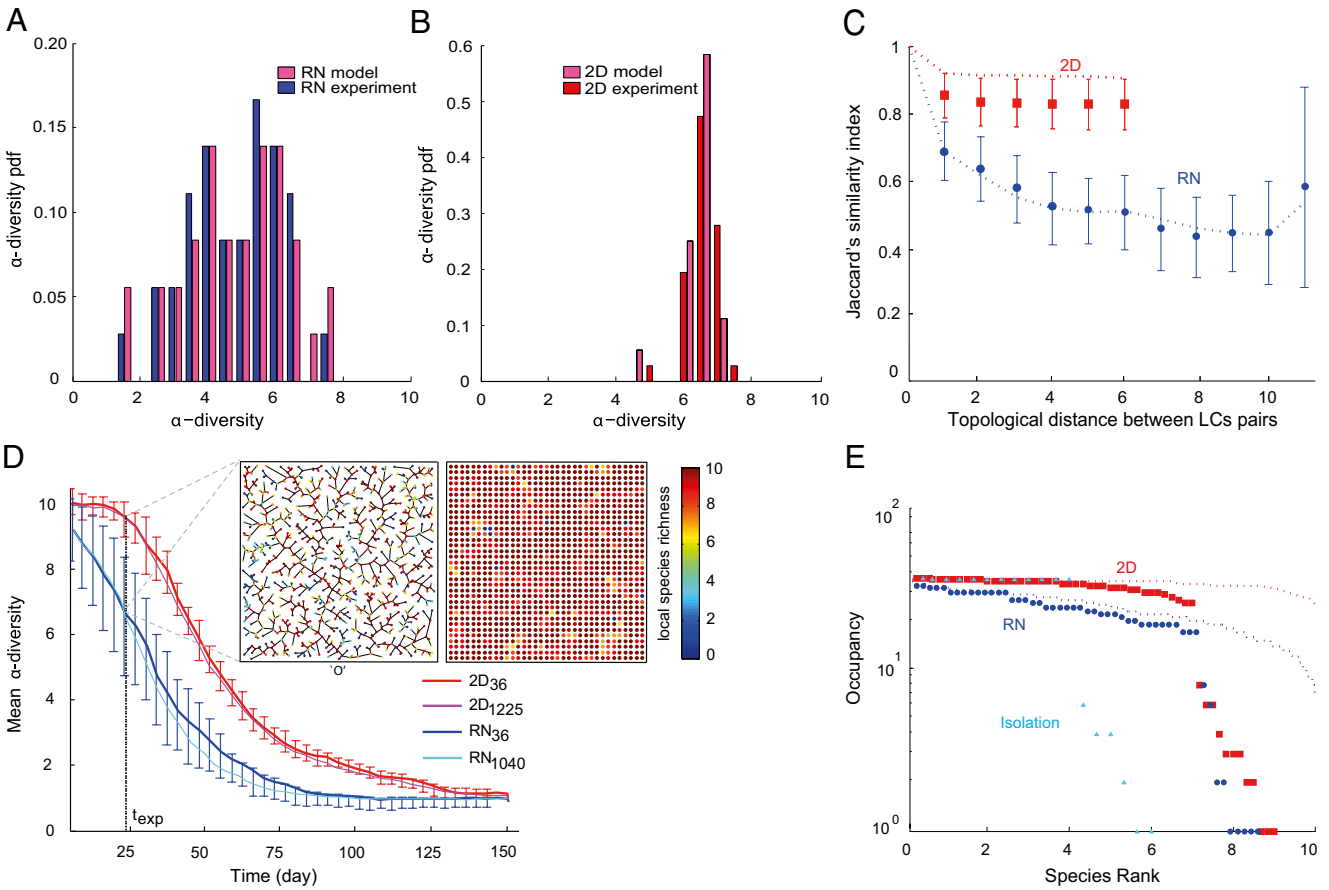

Fig. 3. (*A* and *B*) Probability density function (pdf) of α-diversity for RN and 2D landscapes, with model distributions rescaled to experimental averages. (*C*) β-diversity (JSI) in 2D (red) and in RN (blue), as a function of topological distance between LC pairs (mean ± SD of experimental data, dotted lines are model predictions). The maximum geodesic distance obtained in a 36-site lattice landscape is 6 (in units of topological distance) in the 2D landscape and 11 in the RN. (*D*) Predicted time behavior of mean ± SD α-diversity for RN and 2D at two landscape sizes (36 and 1,040 LCs for RN and 36 and 1,225 LCs for 2D). (*Upper Inset*) α-diversity at t_{exp} = 24 d (black dashed line gives the experimentally measured time point) for a 1,040 LCs RN landscape (O is the outlet) and for a 1,225 LCs 2D landscape. (*E*) Rank-occupancy curve (red for 2D, blue for RN, and cyan for isolation): dotted lines are model predictions. Note the sharp decrease in occupancy for some protozoan species that the model does not predict, indicating stronger competition in the experiment (*SI Materials and Methods*).

Disturbance–Dispersal Events. Spatiotemporal heterogeneity was introduced by disturbance–dispersal events: Twice a week a disturbance–dispersal event was set up, six times in total. Each time, we randomly selected 15 patches to be disturbed per MC. We independently selected these patches for each of the six replicates, but paired one RN and one 2D landscape to be disturbed along the same pattern. The total number of links between the two treatments is different by construction, but the per site amount of dispersal is kept constant. A disturbance event consisted of the removing of all 10 mL of medium present in the LC. After each disturbance event, dispersal was accomplished by manual transfer of 2 ml of medium from every single LC to its nearest neighbors, without bias in directionality (isotropic dispersal), and happened simultaneously in well-mixed conditions, avoiding long-tailed dispersal events (*SI Materials and Methods*). This particular type of density-independent (diffusive) dispersal imposes equal per capita dispersal rates for all different species, and no competition–colonization trade-offs occur (41, 42). We also ran three MC replicates (108 LCs) without any disturbance–dispersal events to test species' coexistence in isolation (isolation treatment, Fig. S7).

Biodiversity Patterns. On day 24, after six disturbance–dispersal treatments, we checked for species presence or absence in each LC. We screened the entire LC under a stereomicroscope, to avoid false absences of the rarer species, obtaining the number of species present in every LC (α-diversity). Because of the nature of the last disturbance event, a few LCs could not be immediately recolonized by neighboring communities. We then determined the spatial distribution of α-diversity and the number of LCs in which a species is present (species occupancy). To characterize β-diversity we considered the spatial decay of Jaccard's similarity index (JSI), defined as $S_{ij}/(S_i + S_j - S_{ij})$, where S_{ij} is the number of species present in both LCs *i* and *j*, whereas S_i is the total number of species in LC *i*. We considered the topological, rather than the Euclidean, distances between community pairs, because they represent the effective distance an individual has to disperse. The notation in the main text $\langle\cdot\rangle$ means a spatial average, whereas the $\bar{\cdot}$ represents an average over the six experimental replicates.

Species' Traits: Size Distribution. We measured the protozoans with a stereomicroscope (Olympus *SZX*16), on which a camera was mounted (*DP*72), and analyzed photographs via software (*cell^D* 3.2). Exposure time and the magnification were optimized for each species. We measured the length of 50 individuals of each species (longest body axis) to get size distributions (Table S1).

Species' Traits: Population Growth. For the growth experiment we cultivated protozoans in pure cultures at identical conditions used for the metacommunity experiment. Population density $\phi(t) = \langle n(t)\rangle/V$ grows in time following the Malthus–Verhulst differential equation (logistic curve)

$$\frac{d\phi_s}{dt} = r_s\phi_s\left(1 - \frac{\phi_s}{K_s}\right), \quad [1]$$

where $s = 1, \ldots, 10$ is the species index, which has the solution

$$\phi_s(t) = \frac{\phi_{0,s}K_s e^{r_s t}}{K_s - \phi_{0,s}(1 - e^{r_s t})}, \quad [2]$$

where $\phi_{0,s}$ is the initial number of individuals per milliliter of medium, for species *s*. For every species we measured the population growth curve in

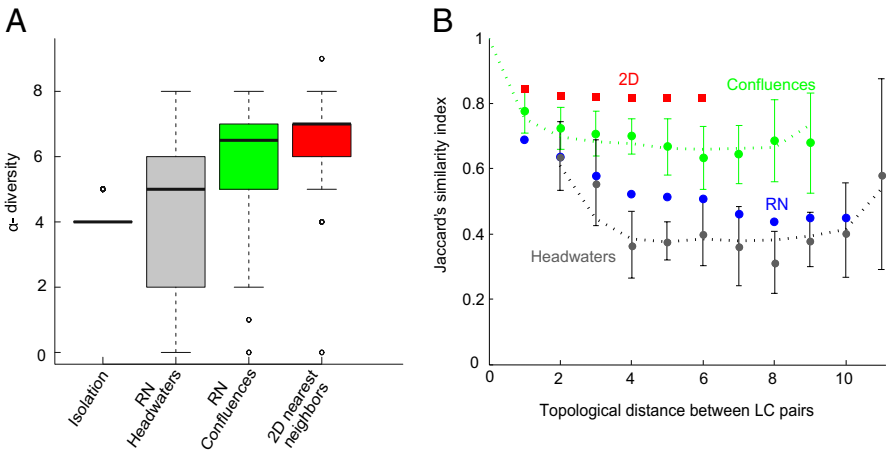

Fig. 4. (*A*) Experimentally observed α-diversity as a function of the degree of connectivity (*d*), e.g., the number of connected neighboring nodes to a LC. For LCs in isolation treatment, $d = 0$; in RN confluences (Cs) have $d = 3$ and headwaters (Hs) have $d = 1$; whereas in 2D all LCs have $d = 4$. Larger *d* results in significantly higher species richness. Boxes represent the median and 25th/75th percentile, and whiskers extend to 1.5 times the interquartile range. (*B*) JSI for Cs (green) and for Hs (black) separately. Solid symbols represent the mean ± SD of the experimental data and dotted lines the model predictions. For comparison, JSI for the entire RN (blue) and for the 2D (red) are shown.

time, averaging over six replicates. We started every replica at the same low density. We measured densities daily for the first 3 d, and subsequently we took measurements depending on the species' growth rate r_s, till saturation of the curve, i.e., carrying capacity K_s. Fig. S3 illustrates the *Colpidium* growth curve with the logistic fit. The complete results for all species are shown in Table S1.

Stochastic Model. The stochastic formulation of the logistic process (the one-step "birth and death process" with space/food limitation) (43) is necessary when volumes of communities and/or number of individuals considered are small. Each individual has a natural death rate *d* and a probability *b* per unit time to produce a second one by division. To ensure that the Markov property holds, *d* and *b* are assumed to be fixed and independent of the age of the individual. Moreover, competition gives rise to an additional death rate $\gamma(n-1)/V$, proportional to the number of other individuals present. For a population of *n* individuals, the transition probabilities read

$$T(n-1|n) = dn + \frac{\gamma}{V}\, n(n-1) \qquad [3]$$

$$T(n+1|n) = bn. \qquad [4]$$

The master equation is

$$\frac{dp_n(t)}{dt} = \left[d(n+1) + \frac{\gamma}{V}(n+1)n\right]p_{n+1}(t) + b(n-1)p_{n-1}(t) - \left[bn + dn + \frac{\gamma}{V}\, n(n-1)\right]p_n(t). \qquad [5]$$

Expansion in *V* (43) gives the macroscopic equation for concentration $\phi = \langle n\rangle/V$,

$$\frac{d\phi}{dt} = (b-d)\phi - \gamma\phi^2, \qquad [6]$$

in which we clearly recognize the logistic equation, provided we identify the macroscopic carrying capacity *K* with $(b-d)/\gamma$, which is the metastable stationary solution ϕ^s for $\phi(t) = \langle n(t)\rangle/V$. We selected a time t_1 such that $n_0 e^{(b-d)t_1}$ is of order $\sqrt{V}$, and for time $t < t_1$ the nonlinear competition term in the master equation is of order $V^{-1/2}$ and may be neglected. The population is simply in its exponential Malthusian growth phase $\langle n(t)\rangle = n_0 e^{(b-d)t}$ and $\langle n^2\rangle - \langle n\rangle^2 = n_0 \frac{b+d}{b-d}[e^{2(b-d)t} - e^{(b-d)t}]$. To disentangle the two factors *b* and *d* hidden inside the macroscopic growth rate $r = b - d$, we performed an analysis of variance among our six experimental replicates: By calculating the macroscopic $\langle n(t)\rangle$ and the variance $\sigma^2(t)$ for time $t < t_1$, we can infer *b* and *d* separately, knowing their sum and difference. The natural death rate for our protist species is $d_s \sim 0$.

Metacommunity Model. We generalize the above arguments to the case of multiple species living in a patchy environment and competing for the same resources. The following discussion is valid for the LC *k* into the whole metacommunity. The nearest-neighbors dispersal along the network is also simulated in a stochastic fashion. We cannot assume "well-mixed" conditions for individuals of all species, so we ideally divide each LC into 100 cells and we randomly distribute individuals in each of these cells. Then we randomly choose 20 cells to be dispersed to the LC's nearest neighbors (same experimental dispersal rate). The most conservative choice—in a pure competition for space framework among individuals of different species—is to consider the following null hypothesis. The competition term $\gamma_i(n_i-1)/V \approx r_i(n_i-1)/(K_i V)$, valid for species *i* in pure growth, changes when taking into account the fact that the fraction of space occupied by an individual of species *j* is K_j/K_i times that of individual of species *i*. The transition probabilities for the birth and the death of an individual of the *i*th species, within a community with $\vec{n} = (n_1, n_2, \ldots, n_i, \ldots, n_S)$ individuals in species pool $P = (1, 2, \ldots, i, \ldots, S)$, respectively, read

$$T(\vec{n} + \vec{e_i}|\vec{n}) = b_i n_i \qquad [7]$$

$$T(\vec{n} - \vec{e_i}|\vec{n}) = d_i n_i + \frac{(b_i - d_i)n_i}{V}\left(\sum_{j\neq i}\frac{n_j}{K_j} + \frac{n_i - 1}{K_i}\right), \qquad [8]$$

where $\vec{e_i}$ is a unit vector whose only *i*th component is not zero. The transition probabilities, when $d_i \equiv 0$, $\forall i \in P$, simplify to

$$T(\vec{n} + \vec{e_i}|\vec{n}) = r_i n_i \qquad [9]$$

$$T(\vec{n} - \vec{e_i}|\vec{n}) = \frac{r_i n_i}{V}\left(\sum_{j\neq i}\frac{n_j}{K_j} + \frac{n_i - 1}{K_i}\right). \qquad [10]$$

The multivariate master equation (43) for the community is given by ref. 44:

$$\frac{\partial p(\vec{n}, t)}{\partial t} = \sum_i \{T(\vec{n}|\vec{n} + \vec{e_i})p(\vec{n} + \vec{e_i}, t) + T(\vec{n}|\vec{n} + \vec{e_i})p(\vec{n} - \vec{e_i}, t) - [T(\vec{n} + \vec{e_i}|\vec{n}) + T(\vec{n} - \vec{e_i}|\vec{n})]p(\vec{n}, t)\}. \qquad [11]$$

The resulting equation for the first moments is

$$\frac{d\langle n_i\rangle}{dt} = r_i\left(\langle n_i\rangle - \sum_{j=1}^{S=10}\frac{\langle n_i n_j\rangle}{K_j V}\right), \qquad [12]$$

which depends also on the second moments. Due to the limited LC volume $V = 10$ mL and the fact that the species' carrying capacity in some cases is small (<100 individuals per milliliter of medium), fluctuations around the

ECOLOGY

macroscopic solutions may not be negligible. Thus, we performed numerical simulations using the Gillespie algorithm (45), which allows us to produce time series that exactly recover the solution of the multivariate master equation in Eq. **11** with transition probabilities in Eqs. **9** and **10**. Edge effects in the lattice landscape are removed by imposing periodic boundary conditions. The dynamics of the system are stochastically perturbed to include diffusive dispersal of individuals across patches and spatially uncorrelated environmental disturbances, reflecting the experimental conditions. A simulation ends when the system has reached monodominance. Actually, in the experimental disturbance regime (and without any speciation process taken into account), only the species with the highest growth rate survives in the simulations.

ACKNOWLEDGMENTS. We thank E. Bertuzzo, T. Fukami, M. Gatto, A. Giometto, L. Mari, and A. Maritan for invaluable help, support, comments, and suggestions. We also thank F. de Alencastro (CEAL/IIE/École Polytechnique Fédérale Lausanne) for generous support. We thank Sophie Campiche for access to laboratory material and R. Illi for protozoan pictures. Funding is from ERC Advanced Grant RINEC 22761 (to A.R. and F.C.), Swiss National Science Foundation Grant 200021/124930/1 (to A.R. and F.C.), and Swiss National Science Foundation Grant 31003A_135622 (to F.A.).

1. Sheldon AL (1968) Species diversity and longitudinal succession in stream fishes. *Ecology* 49:193–198.
2. Hastings A, Higgins K (1994) Persistence of transients in spatially structured ecological models. *Science* 263:1133–1136.
3. Urban D, Keitt T (2001) Landscape connectivity: A graph-theoretic perspective. *Ecology* 82:1205–1218.
4. Fagan WF (2002) Connectivity, fragmentation, and extinction risk in dendritic metapopulations. *Ecology* 83:3243–3249.
5. Holyoak M, Leibold MA, Holt RD (2005) *Metacommunities. Spatial Dynamics and Ecological Communities* (Univ of Chicago Press, Chicago).
6. Campbell Grant EH, Lowe WH, Fagan WF (2007) Living in the branches: Population dynamics and ecological processes in dendritic networks. *Ecol Lett* 10:165–175.
7. Muneepeerakul R, et al. (2008) Neutral metacommunity models predict fish diversity patterns in Mississippi-Missouri basin. *Nature* 453:220–222.
8. Bertuzzo E, et al. (2011) Spatial effects on species persistence and implications for biodiversity. *Proc Natl Acad Sci USA* 108:4346–4351.
9. Hubbell SP (2001) *The Unified Theory of Biodiversity and Biogeography* (Princeton Univ Press, Princeton).
10. Volkov I, Banavar JR, He F, Hubbell SP, Maritan A (2005) Density dependence explains tree species abundance and diversity in tropical forests. *Nature* 438:658–661.
11. de Aguiar MAM, Baranger M, Baptestini EM, Kaufman L, Bar-Yam Y (2009) Global patterns of speciation and diversity. *Nature* 460:384–387.
12. Levine JM, HilleRisLambers J (2009) The importance of niches for the maintenance of species diversity. *Nature* 461:254–257.
13. Rodriguez-Iturbe I, Rinaldo A (1997) *Fractal River Basins: Chance and Self-Organization* (Cambridge Univ Press, New York).
14. Benda L, et al. (2004) The network dynamics hypothesis: How channel networks structure riverine habitats. *Bioscience* 54:413–427.
15. Madin JS, Connolly SR (2006) Ecological consequences of major hydrodynamic disturbances on coral reefs. *Nature* 444:477–480.
16. Fernandes CC, Podos J, Lundberg JG (2004) Amazonian ecology: Tributaries enhance the diversity of electric fishes. *Science* 305:1960–1962.
17. Cardinale BJ, Hillebrand H, Charles DF (2006) Geographic patterns of diversity in streams are predicted by a multivariate model of disturbance and productivity. *J Ecol* 94:609–618.
18. Clarke A, Mac Nally R, Bond N, Lake PS (2008) Macroinvertebrate diversity in headwater streams: A review. *Freshw Biol* 53:1707–1721.
19. Fér T, Hroudová Z (2008) Detecting dispersal of nuphar lutea in river corridors using microsatellite markers. *Freshw Biol* 53:1409–1422.
20. Warren PH (1996) Dispersal and destruction in a multiple habitat system: An experimental approach using protist communities. *Oikos* 77:317–325.
21. Haddad NM, et al. (2008) Species' traits predict the effects of disturbance and productivity on diversity. *Ecol Lett* 11:348–356.
22. Altermatt F, Schreiber S, Holyoak M (2011) Interactive effects of disturbance and dispersal directionality on species richness and composition in metacommunities. *Ecology* 92:859–870.
23. Altermatt F, Bieger A, Carrara F, Rinaldo A, Holyoak M (2011) Effects of connectivity and recurrent local disturbances on community structure and population density in experimental metacommunities. *PLoS ONE*, 10.1371/journal.pone.0019525.
24. Jessup CM, et al. (2004) Big questions, small worlds: Microbial model systems in ecology. *Trends Ecol Evol* 19:189–197.
25. Fukami T (2001) Sequence effects of disturbance on community structure. *Oikos* 92: 215–224.
26. Gonzalez A, Lawton JH, Gilbert FS, Blackburn TM, Evans-Freke I (1998) Metapopulation dynamics, abundance, and distribution in a microecosystem. *Science* 281: 2045–2047.
27. Cadotte MW (2006) Metacommunity influences on community richness at multiple spatial scales: A microcosm experiment. *Ecology* 87:1008–1016.
28. Matthiessen B, Hillebrand H (2006) Dispersal frequency affects local biomass production by controlling local diversity. *Ecol Lett* 9:652–662.
29. Fukami T, Morin PJ (2003) Productivity-biodiversity relationships depend on the history of community assembly. *Nature* 424:423–426.
30. Fukami T, et al. (2010) Assembly history dictates ecosystem functioning: Evidence from wood decomposer communities. *Ecol Lett* 13:675–684.
31. Holyoak M, Lawler SP (2005) Population dynamics and laboratory ecology. *Advances in Ecological Research* (Academic Press, London), Vol 37, pp 245–271.
32. Muneepeerakul R, Weitz JS, Levin SA, Rinaldo A, Rodriguez-Iturbe I (2007) A neutral metapopulation model of biodiversity in river networks. *J Theor Biol* 245:351–363.
33. Morrissey MB, de Kerckhove DT (2009) The maintenance of genetic variation due to asymmetric gene flow in dendritic metapopulations. *Am Nat* 174:875–889.
34. Newman MEJ (2010) *Networks* (Oxford Univ Press, Oxford).
35. Brown BL, Swan CM (2010) Dendritic network structure constrains metacommunity properties in riverine ecosystems. *J Anim Ecol* 79:571–580.
36. Damschen EI, Haddad NM, Orrock JL, Tewksbury JJ, Levey DJ (2006) Corridors increase plant species richness at large scales. *Science* 313:1284–1286.
37. Cadotte MW (2006) Dispersal and species diversity: A meta-analysis. *Am Nat* 168: 913–924.
38. McGrady-Steed J, Harris PM, Morin PJ (1997) Biodiversity regulates ecosystem predictability. *Nature* 390:162–165.
39. Rodriguez-Iturbe I, et al. (1992) Fractal structures as least energy patterns: The case of river networks. *Geophys Res Lett* 19:889–893.
40. Rinaldo A, et al. (1992) Minimum energy and fractal structures of drainage networks. *Water Resour Res* 28:2183–2191.
41. Cadotte MW, et al. (2006) On testing the competition-colonization trade-off in a multispecies assemblage. *Am Nat* 168:704–709.
42. Cadotte MW (2007) Competition-colonization trade-offs and disturbance effects at multiple scales. *Ecology* 88:823–829.
43. van Kampen NG (2007) *Stochastic Processes in Physics and Chemistry* (North-Holland, Amsterdam).
44. Volkov I, Banavar JR, Hubbell SP, Maritan A (2009) Inferring species interactions in tropical forests. *Proc Natl Acad Sci USA* 106:13854–13859.
45. Gillespie DT (1977) Exact stochastic simulation of coupled chemical-reactions. *J Phys Chem* 81:2340–2361.

Supporting Information

Carrara et al. 10.1073/pnas.1119651109

SI Materials and Methods

Disturbance–Dispersal Events. In this section we describe in detail the experimental protocol for the microcrosm metacommunities.

Fig. 1*B* in the main text shows the following species: *Blepharisma* sp., *Euglena gracilis*, *Cephalodella* sp. (*Upper* row from *Left* to *Right*), *Paramecium bursaria*, *Colpidium*, and *Spirostomum* sp. (Lower row from *Left* to *Right*). In Table S1 we summarize the species' traits for our species pool.

A disturbance event consisted of the removing of all 10 mL of medium present in the local community (LC). To test the effectiveness of disturbance, one metacommunity (MC) experienced disturbances but no dispersal. In this treatment, we found the persistence of two species in only 1 LC (of 36 LCs): *Cephalodella* sp. and *Tetrahymena* sp. Thus, we conclude that disturbance events were highly effective.

After each disturbance event, dispersal was accomplished by manual transfer from every single LC to its nearest neighbors, without bias in directionality (isotropic dispersal). We applied the following dispersal procedure:

We thoroughly mixed the medium in every undisturbed LC.
We transferred from each LC in total 2 mL (20%) of medium to its nearest neighbors along the respective network on a "mirror" landscape of 36 empty plates (Fig. S1). We chose boundary conditions in which headwaters dispersed only one-third of medium (~0.67 mL) dispersed by confluences in the river network (RN) and LCs in 2D landscapes.
We collected and mixed dispersed medium in mirror landscapes.
We retransferred to the "real" landscape.
We filled up every LC to 10 mL with fresh medium.

In this manner the dispersal happened simultaneously in well-mixed conditions, and we avoided long-tailed dispersal events. We point out that, by construction, the total number of links between the two treatments is different, but the per site amount of dispersal has been kept constant (see above). This particular type of density-independent (diffusive) dispersal, imposing equal per capita dispersal rates for all different species and no competition–colonization trade-offs (1, 2), singles out the effects of connectivity on biodiversity patterns, having fixed the per site dispersal.

"Isolation" Treatment. We also ran three MC replicates (108 LCs) without any disturbance–dispersal events to test species coexistence in isolation (isolation treatment). To avoid excessive deterioration of the medium in these isolated communities, on day 12 we replaced 20% of old medium with fresh sterile medium. Fig. S7 shows the three replicates for the isolation treatment. We have already noted in the main text that competition for resources and predation clearly disadvantaged certain species. We experimentally proved that, starting from the same initial conditions, only the same subset of species (*Cephalodella* sp. and the three photosynthetic ones, see Fig. S7 and Table S1 for species' traits) can persist without any kind of perturbation event.

Competitive Exclusion Dynamics. A temporal analysis of the disturbance events permits us to isolate the species that shows a disturbance-dependent behavior (3). Every LC has a different "disturbance history." We divide LCs in classes, in which every LC in a class has the same time from the last disturbance event, and we obtain the species occupancy distribution for these classes. If a species has a nonsensitive behavior to disturbances, its distribution should be constant over the different disturbance classes. This temporal analysis is strictly linked to competition rank: If a species is rarely found in a LC that has been disturbed long ago, it is very likely that its competition rank is low and vice versa. Fig. S6 shows that smaller species (*Chilomonas*, *Tetrahymena*, and *Colpidium* sp.) that have high growth rates and carrying capacities are almost absent in LC classes disturbed long ago and therefore have low competition rank. These smaller species have never been found in the communities at the end of the isolation treatment. Thus, the spatiotemporal heterogeneity induced by disturbance and dispersal events has prevented competitive exclusion dynamics, which would have excluded the weaker species in long-term regimes. We note that the subset of disadvantage species, as expected, was consistent across experimental replicates.

Stochastic Metacommunity Model. The volume of medium per community is relatively small ($V = 10$ mL), and for some species the carrying capacities can be under hundreds individuals per milliliter (Table S1). In such situations fluctuations around the concentration $\phi(t)$ may not be negligible at all, playing instead a significant role in the dynamics of the process (4). A stochastic description of the growth process is therefore required to obtain more reliable results.

The deterministic solution provided in *Materials and Methods* in the main text (Fig. S3 shows the *Colpidium* growth curve) is a good approximation for high-density species and for a large volume V of medium. V denotes the available space that can be occupied by protozoans and bacteria. We considered the following facts:

Bacteria species are at least one order of magnitude smaller than the smallest protozoan species in our experiment.
Bacteria carrying capacities are of the order of millions per milliliter.
Bacteria growth rates are at least 10-fold higher than protozoan growth rates.

We thus decided not to include bacteria dynamics in our model, assuming that their abundance may be considered constant at the timescale of protozoan dynamics.

The experiments ended at day 24, after six disturbance–dispersal events. On day 24 we collected data on presence or absence of metacommunity species, observing different biodiversity patterns resulting from long-term community dynamics for the RN and 2D landscapes. However, what about the patterns at different timescales? Our combined approach of the microcosm experiments with the metacommunity model let us answer this important question (5). Actually, having verified that the model predicts the biodiversity patterns at one particular time point, we can easily control the behavior of the system at different timescales (Fig. 3*D* of the main text and Fig. S4). The dynamics of the system, stochastically perturbed to include diffusive dispersal of individuals across patches and spatially uncorrelated environmental disturbances, reflects the experimental conditions. A simulation ends when the system has reached monodominance; i.e., only one species survives in the metacommunity. Actually, in the experimental disturbance regime, having considered in our model neither speciation processes (6) nor niche differences (7), only the species with the highest growth rates survive in the simulations. We verified that the patterns hold in this entire time interval, whereas the average $\langle\alpha\rangle$-diversity for the two landscapes decreases consistently in time (Fig. 3*D*). Fig. S4 shows the biodiversity patterns compared in the main text for the two landscapes, at different time points. The system is predicted to be in a long transient

state. We confirmed that our experimental results are general over ecologically important timescales, meaning that the timescales are large relative to species generation time. Actually, the time interval in which the system has been analyzed corresponds to ~50–300 generations, depending on the species' growth rate (Table S1).

Modeling Riverine Ecosystem Connectivity. Our replicated and controlled experimental design sheds light on connectivity in driving important biodiversity patterns of simplified metacommunities, disentangling complex natural systems' behavior (5). We decided to study such basic mechanisms in river network geometry as an important benchmark. To generally describe topological and metric properties of river network connectivity, we reproduce stationary states of the general landscape evolution equation through the static model known as the optimal channel network (OCN) (see refs. 8 and 9 for a review). The OCN model was originally based on the ansatz that configurations occurring in nature are those that minimize a functional describing the dissipated energy and on the derivation of an explicit form for such a functional. A later proof (10, 11) confirmed that optimal networks are exactly related to the stationary solutions of the basic landscape evolution equation to leading order in the small gradient approximation. In particular, any configuration that minimizes total energy dissipation, within the framework of general dynamical rules, corresponds, through a slope-discharge relation, to an elevation field that is a stationary solution of the basic landscape evolution equation. Thus, spanning, loopless network configurations characterized by minimum energy dissipation are obtained by selecting the configuration, say s, that minimizes

$$E(s) = \sum_j a_j^{\gamma}, \qquad \textbf{[S1]}$$

where j spans the lattice and $a_i = \sum_j W_{j,i} a_j + 1$ is the value of the drainage area $a_i\ \forall i$. $W_{j,i}$ is the element of the connectivity matrix spanning all nodes and determining uniquely, in a spanning loopless tree. The exponent γ is exactly $\gamma = 1/2$ in the small gradient approximation and it is crucial that one has $\gamma < 1$ from the physics of the problem (11).

The global minimum (the ground state) of the functional in Eq. **3** is exactly characterized by known mean field exponents. Thus, any stationary solution of the landscape evolution equation must locally satisfy the slope–area relationship.

The 3D drainage basin can be reconstructed using the rule of steepest descent; that is, the flux at a point j has the direction of the maximum gradient of the elevation field (the direction toward the lowest among all nearest neighbors to j). Moreover, the channelized part of the landscape is necessarily (but not sufficiently) identified by topographically concave areas where the above assumption holds strictly. Thus, one can uniquely associate any landscape with an oriented spanning graph on the lattice, i.e., an oriented loopless graph passing through each point. Identifying the flux in a point i with the total area a_i drained in that point, one can reconstruct the field of landscape-forming fluxes corresponding to a given oriented spanning graph. From the fluxes, a field of elevation can be defined using the above relation with the local slope.

Fig. 1*A* shows a local minimum of E in Eq. **3**, obtained by moving from an initial configuration s. A site is then chosen at random, and the connectivity W (hence the configuration s) is perturbed by disconnecting a link, which is reoriented to produce a new configuration s'. If the new configuration lowers total energy dissipation, i.e., $E(s') \leq E(s)$, the change is accepted and the procedure is restarted. Fig. 1*A* is obtained through the same procedure where an annealing procedure has been implemented; i.e., unfavorable changes may also be accepted with probability $\propto \exp(-[E(s) - E(s')]/T)$, where T assumes the role of temperature in a gas or a spin glass. Only changes that retain the loopless character are retained because every local minimum of the functional (3) is a tree (11–13). Iteration to convergence in the connectivity structure W thus produces the desired planar and 3D landforms. The final number of nodes in the network is obtained by considering from the original space-filling configuration (all pixels in the landscape domain are channelized) only those nodes with a drainage area $a_i > a_t$, where a_t denotes an adequate threshold.

In network theory, an important measure of centrality is provided by the closeness centrality, defined as the average of the inverse distances from a vertex to other vertices:

$$C_i = \frac{1}{n-1} \sum_{(j \neq i)} \frac{1}{d_{ij}}. \qquad \textbf{[S2]}$$

It is directly related to the "ecological diameter" l_i, defined in the main text, which measures the mean distance from a LC to all other LCs. Fig. S2 shows the ecological diameter distribution for the RN (in a 36-lattice landscape it is simply a delta function on $l_i^{2D} = l^{2D} = 3$).

For the statistical analysis, as indicated in the main text, we performed paired t tests to compare values from the six replicates for the RN and 2D treatments. Fig. S5 shows the cumulative probability function of α-diversity for the different connectivity classes. For the analysis in the RN, we performed an ANOVA with connectivity d, disturbance, and ecological diameter l_i as factors (see main text), with random effects, due to the six different replicates. We identified seven classes of disturbance, according to the time to the last disturbance event to which a LC has been subjected. Actually, at the measurement time, the MCs have been exposed to six disturbance–dispersal events, but each LC exhibited different disturbance treatments (see *Materials and Methods* in the main text for disturbance protocol). In the class "0" a LC has been subjected to the last disturbance, and in the class "6" a LC has never been disturbed. We rounded l_i to the nearest integer, thus identifying five classes (3–7) for the ecological diameter.

1. Cadotte MW, et al. (2006) On testing the competition-colonization trade-off in a multispecies assemblage. *Am Nat* 168:704–709.
2. Cadotte MW (2007) Competition-colonization trade-offs and disturbance effects at multiple scales. *Ecology* 88:823–829.
3. Haddad NM, et al. (2008) Species' traits predict the effects of disturbance and productivity on diversity. *Ecol Lett* 11:348–356.
4. Melbourne BA, Hastings A (2008) Extinction risk depends strongly on factors contributing to stochasticity. *Nature* 454:100–103.
5. Holyoak M, Lawler SP (2005) Population dynamics and laboratory ecology. *Adv Ecol Res* 37:245–271.
6. Hubbell SP (2001) *The Unified Theory of Biodiversity and Biogeography* (Princeton Univ Press, Princeton).
7. Chesson P (2000) Mechanisms of maintenance of species diversity. *Annu Rev Ecol Syst* 31:343–366.
8. Rinaldo A, Rigon R, Rodriguez-Iturbe I (1999) Channel networks. *Annu Rev Earth Planet Sci* 26:289–306.
9. Rinaldo A, Banavar JR, Maritan A (2006) Trees, networks and hydrology. *Water Resour Res*, 10.1029/2005WR004108.
10. Banavar JR, et al. (1997) Sculpting of a fractal river basin. *Phys Rev Lett* 78:4522–4526.
11. Banavar JR, Colaiori F, Flammini A, Maritan A, Rinaldo A (2001) Scaling, optimality and landscape evolution. *J Stat Phys* 104:1–33.
12. Banavar JR, Maritan A, Rinaldo A (1999) Size and form in efficient transportation networks. *Nature* 399:130–132.
13. Banavar JR, Colaiori F, Flammini A, Maritan A, Rinaldo A (2000) Topology of the fittest transportation network. *Phys Rev Lett* 84:4745–4748.

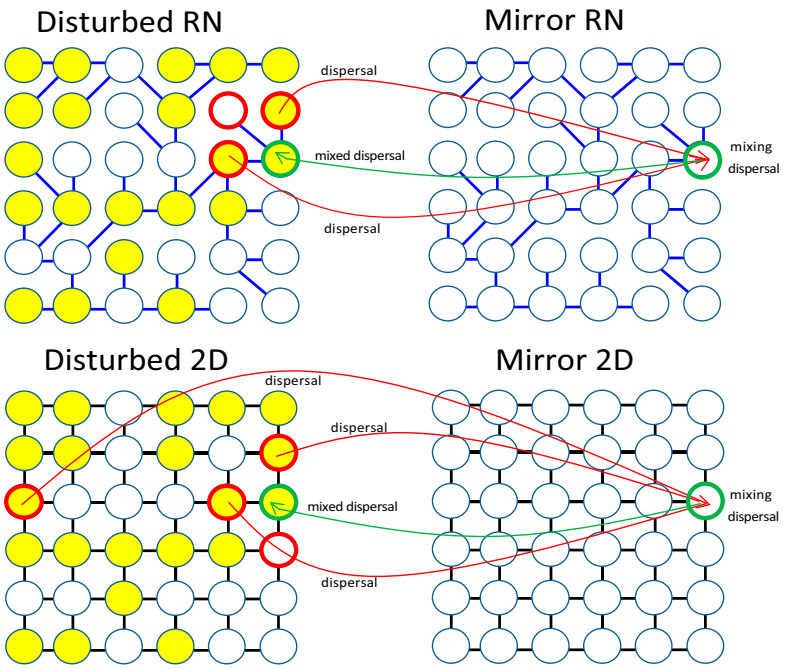

Fig. S1. Dispersal protocol for the RN and 2D treatments. In this example we show the first replicate and the sixth disturbance event. Yellow circles represent undisturbed LCs (the same for RN and 2D). We transferred migrants from every undisturbed LC to its nearest neighbor(s) in a "mirror" landscape, where we mixed the migrants. Then we dispersed them back to the original position in a "real" landscape. Following this procedure the dispersal happened simultaneously. Throughout, we show the dispersal for red LC migrants from green LC neighborhoods for RN (closest upstream and downstream LCs) and 2D (four nearest neighbors, periodic boundaries) landscapes.

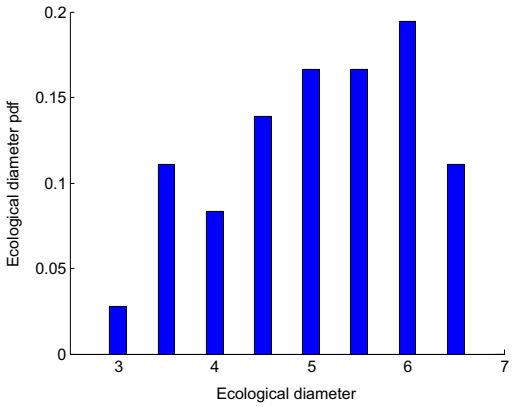

Fig. S2. The probability density function (pdf) for the ecological diameter l_i for the RN landscape. In a 36-lattice landscape it is a delta function on $l_i^{2D} = l = 3$.

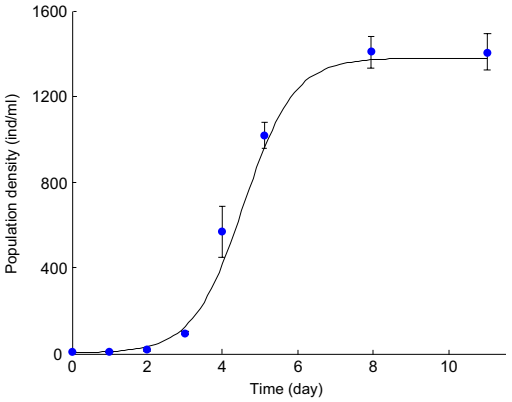

Fig. S3. Population growth curve for *Colpidium* sp. obtained in the same conditions as the metacommunity experiment. Average ± SD is shown of six experimental replicates (blue points) and logistic fit (black line).

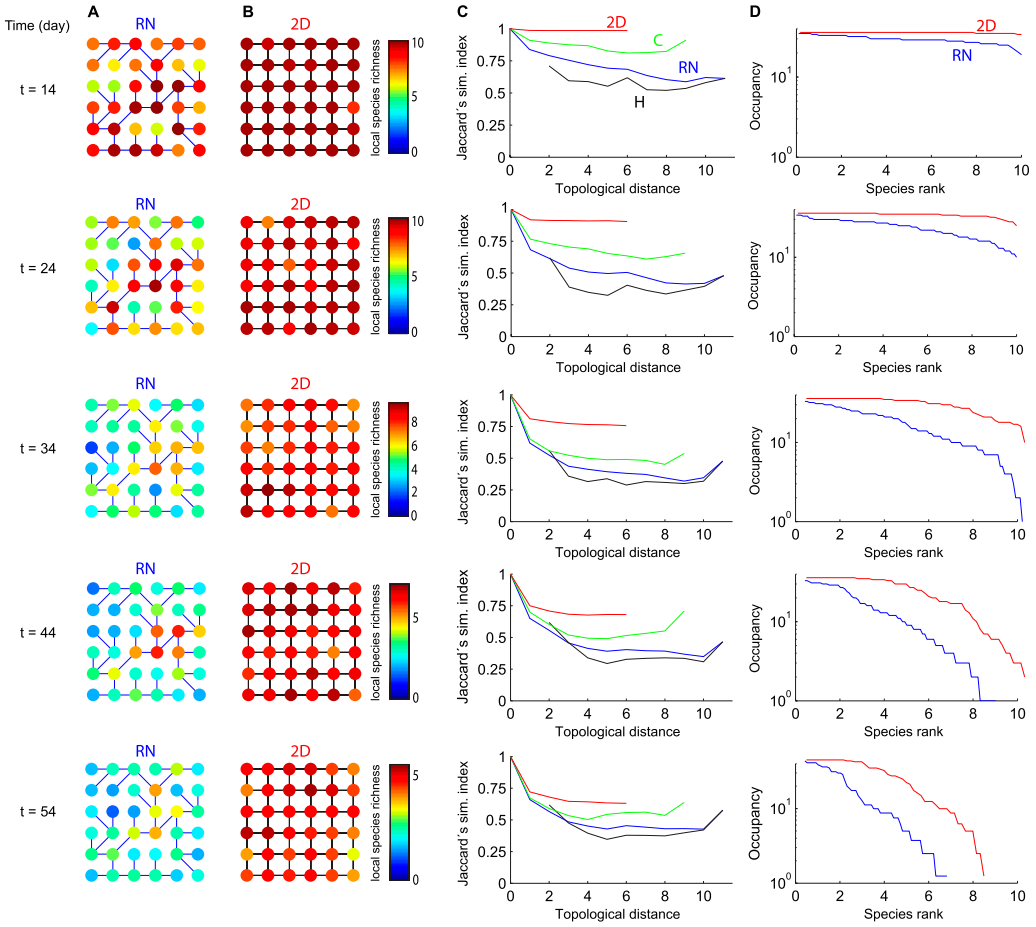

Fig. S4. Time behavior of biodiversity patterns in RN and 2D landscapes. (*A*–*D*) Average α-diversity (*A* and *B*), β-diversity (*C*), and rank-occupancy curve (*D*) at different time points are shown. The patterns found in the experiment at t_{exp} = 24 d (Fig. 2) are maintained for a long time interval in the stochastic metacommunity model. Moreover, in the isolation experiment, we show that over temporal scales $t \sim t_{exp}$ the communities are driven by competition–exclusion dynamics to a lower biodiversity state (Fig. S7).

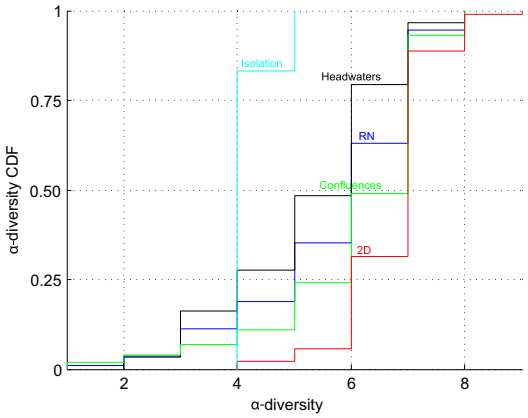

Fig. S5. Cumulative density function (CDF) of α-diversity for different landscapes. The α-diversity CDF is shown by red and blue lines for 2D and RN, black lines for headwaters, green lines for confluences, and cyan lines for isolation.

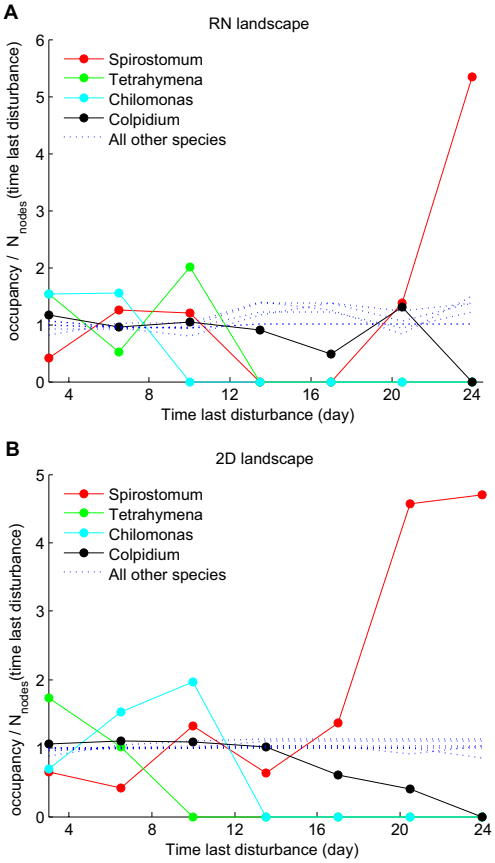

Fig. S6. Impact of disturbance events on species persistence. (*A* and *B*) Distribution of species occupancies is shown relative to the temporal distribution of disturbance events in RN (*A*) and 2D (*B*) landscapes. Solid symbols represent deviations from a nonsensitive behavior to disturbance (dotted blue lines). We found that smaller protozoans (*Chilomonas* sp., *Tetrahymena* sp., and *Colpidium* sp., respectively cyan, green, and black) occupied only sites that had been recently disturbed, suggesting that these species were competitively inferior. We observed opposite behavior for *Spirostomum* sp. (red), which predominantly occupied patches that were disturbed relatively long ago.

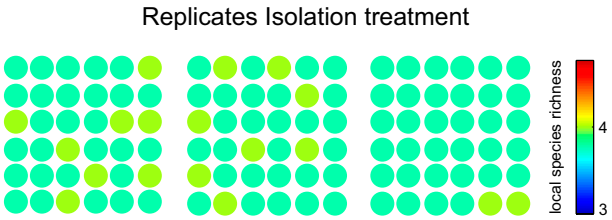

Fig. S7. α-diversity for the three replicates of the aquatic microcosm communities in the isolation treatment. Specifically, *Euglena gracilis*, *Euplotes aediculatus*, *Paramecium bursaria*, and *Cephalodella* sp. survived in all LCs of the three MCs, whereas *Paramecium aurelia* and *Blepharisma* sp. survived in a small fraction of them. Compare absolute numbers for local species richness (color coded) with Fig. 2 *C* and *D* of the main text.

Table S1. Experimentally measured species' traits (mean ± SD)

Species	Size, μm	Growth rate *r*, 1/d	Carrying capacity *K*, ind/mL
Blepharisma	471.3 ± 57.1	0.67 ± 0.07	59.5 ± 4.7
Cephalodella	112.7 ± 11.2	0.67 ± 0.11	902.8 ± 121.8
Chilomonas	23.3 ± 3.7	0.98 ± 0.13	1,572.4 ± 278.3
Colpidium	81.0 ± 7.8	1.50 ± 0.08	1,379.2 ± 76.6
*E. gracilis**	36.7 ± 6.4	0.87*	84,578[†]
*E. aediculatus**	85.4 ± 8.6	0.43*	359[†]
*P. bursaria**	101.3 ± 12.9	0.23*	1,639[†]
P. aurelia	111.6 ± 15.1	0.86 ± 0.02	111.1 ± 2.6
Spirostomum	843.8 ± 149.7	0.57 ± 0.15	13.6 ± 4.2
Tetrahymena	26.7 ± 4.8	2.24 ± 0.15	2,996.8 ± 196.1

ind/mL, individuals per milliliter.
*Mixotroph that can eat bacteria and photosynthesize.
[†]Data from ref. 3.